# Formation of diluted III–V nitride thin films by N ion implantation

K. M. Yu, W. Walukiewicz, J. Wu, J. W. Beeman, J. W. Ager III, E. E. Haller, W. Shan, H. P. Xin, C. W. Tu, and M. C. Ridgway

Citation: Journal of Applied Physics **90**, 2227 (2001); doi: 10.1063/1.1388860
View online: http://dx.doi.org/10.1063/1.1388860
View Table of Contents: http://scitation.aip.org/content/aip/journal/jap/90/5?ver=pdfcov
Published by the AIP Publishing

# Formation of diluted III–V nitride thin films by N ion implantation

K. M. Yu,[a] W. Walukiewicz, J. Wu, J. W. Beeman, J. W. Ager III, and E. E. Haller
*Materials Sciences Division, Lawrence Berkeley National Laboratory, Berkeley, California 94720*

W. Shan
*OptiWork, Inc., Fremont, California 94538*

H. P. Xin and C. W. Tu
*Department of Electrical and Computer Engineering, University of California at San Diego, La Jolla, California 92093*

M. C. Ridgway
*Department of Electronic Materials Engineering, Research School of Physical Sciences and Engineering, Australian National University, Canberra, Australia*

(Received 24 January 2001; accepted for publication 4 June 2001)

Diluted III–$N_x$–$V_{1-x}$ alloys were successfully synthesized by nitrogen implantation into GaAs, InP, and $Al_yGa_{1-y}As$. In all three cases the fundamental band-gap energy for the ion beam synthesized III–$N_x$–$V_{1-x}$ alloys was found to decrease with increasing N implantation dose in a manner similar to that observed in epitaxially grown $GaN_xAs_{1-x}$ and $InN_xP_{1-x}$ alloys. In $GaN_xAs_{1-x}$ the highest value of $x$ (fraction of ''active'' substitutional N on As sublattice) achieved was 0.006. It was observed that $N_{As}$ is thermally unstable at temperatures higher than 850 °C. The highest value of $x$ achieved in $InN_xP_{1-x}$ was higher, 0.012, and the $N_P$ was found to be stable to at least 850 °C. In addition, the N activation efficiency in implanted $InN_xP_{1-x}$ was at least a factor of 2 higher than that in $GaN_xAs_{1-x}$ under similar processing conditions. $Al_yGa_{1-y}N_xAs_{1-x}$ had not been made previously by epitaxial techniques. N implantation was successful in producing $Al_yGa_{1-y}N_xAs_{1-x}$ alloys. Notably, the band gap of these alloys remains direct, even above the value of $y$ ($y>0.44$) where the band gap of the host material is indirect. © *2001 American Institute of Physics.* [DOI: 10.1063/1.1388860]

## I. INTRODUCTION

Recently a new class of materials, diluted III–V nitrides (III–$N_x$–$V_{1-x}$) formed by adding a small amount of N (typically less than 5%) to the III–V semiconductor matrix, has generated considerable interest. The first system that has been extensively studied recently was $GaN_xAs_{1-x}$.[1–3] Reduction of the band gap by more than 100 meV per atomic percent of N has been observed in $GaN_xAs_{1-x}$ alloys grown by plasma-assisted metalorganic chemical vapor deposition.[2–4] Comparably large band-gap reductions have also been observed in GaInNAs,[3,5] GaNP,[6,7] InNP,[8] and AlGaNAs.[9] The strong dependence of the band gap on the N content has made diluted III–V nitrides important materials for a variety of applications, including long wavelength optoelectronic devices[10,11] and high efficiency hybrid solar cells.[12,13]

Several theoretical studies have addressed the unusually strong dependence of the fundamental gap on the N content in the group III–N–V alloys.[14–17] Band structure calculations using either density functional theory (DFT) with the local density approximation (LDA)[15] or a combination of LDA and the empirical pseudopotential method[16] have attributed the observed changes in the conduction band structure to N-induced interactions between the extended states of Γ, $L$, and/or $X$ minima.

Recently, Shan *et al.*[18] and Perkins *et al.*[19] have used modulation spectroscopy techniques to observe an additional feature in the optical spectrum of GaInNAs alloys. The onset of the new optical transitions has also been confirmed by direct measurements of the optical absorption on a free standing GaInNAs layer.[20] The appearance of this new absorption edge above the fundamental gap has been attributed to an anticrossing interaction between localized N states and the extended states of the host semiconductor matrix.[18,21] In this band-anticrossing (BAC) model, the interaction splits the conduction band into two subbands. The downward shift of the lower subband is responsible for the reduction of the fundamental band gap and optical transitions from the valence band to the upper subband account for the high-energy edge. The model has been successfully used to quantitatively describe the dependencies of the upper and lower subband energies on hydrostatic pressure and on N content.[21]

In the BAC model, the dispersion relations for the upper and lower conduction subbands are given by

$$E_{\pm}(k)=\tfrac{1}{2}[E_N+E_M(k)\pm\sqrt{[E_N-E_M(k)]^2+4C_{NM}^2x}], \quad (1)$$

where $E_N$ is the energy of the N level, $E_M(k)$ is the dispersion relation for the host semiconductor matrix, and $C_{NM}$ is the matrix element describing the coupling between N states and the extended states. For $GaN_xAs_{1-x}$, the downward shift of the lower subband $E_-$ can account well for the reduction of the fundamental band gap using a value of

[a]Electronic mail: kmyu@lbl.gov

 

TABLE I. Detailed information on the N implantation conditions on the various samples.

| Implant | Implanted N (%) | Implantation temperature | Energy (keV) | Dose (at./cm$^2$) | Total dose (at./cm$^2$) |
|---|---|---|---|---|---|
| N (single implant) | 0.8 | RT | 160 | $4\times10^{15}$ | $6.63\times10^{15}$ |
| | | | 77 | $1.7\times10^{15}$ | |
| | | | 35 | $9.3\times10^{14}$ | |
| | 1.6 | RT | 160 | $8\times10^{15}$ | $1.326\times10^{16}$ |
| | | | 77 | $3.4\times10^{15}$ | |
| | | | 35 | $1.86\times10^{15}$ | |
| | 1.8 | RT | 120 | $6.3\times10^{15}$ | $9.5\times10^{15}$ |
| | | | 60 | $2.4\times10^{15}$ | |
| | | | 35 | $8.0\times10^{14}$ | |
| | 2.0 | RT | 100 | $7.0\times10^{15}$ | $1.03\times10^{16}$ |
| | | | 50 | $2.5\times10^{15}$ | |
| | | | 33 | $8.0\times10^{14}$ | |
| | 3.6 | RT | 120 | $1.26\times10^{16}$ | $1.7\times10^{16}$ |
| | | | 60 | $4.8\times10^{15}$ | |
| | | | 35 | $1.6\times10^{15}$ | |
| | 1.6 | RT | 160 | $2.4\times10^{16}$ | $3.98\times10^{16}$ |
| | | | 77 | $1.02\times10^{16}$ | |
| | | | 35 | $5.58\times10^{15}$ | |
| N (co-implant) | 2.0 | 350 °C | 450 | $1.5\times10^{16}$ | $2.15\times10^{16}$ |
| | | | 255 | $6.5\times10^{15}$ | |
| Ga (co-implant) | 2.0 | 350 °C | 1250 | $2.4\times10^{16}$ | $2.4\times10^{16}$ |
| Al (co-implant) | 2.0 | 350 °C | 450 | $1.7\times10^{16}$ | $2.0\times10^{16}$ |
| | | | 330 | $3\times10^{15}$ | |

$E_N=1.65$ eV above the VB maximum derived from photoluminescence measurements in N-doped GaAs[22] and from fitting the data to obtain $C_{NM}=2.7$ eV.[18,21]

The band anticrossing model predicts that the incorporation of small amounts of N ($\geqslant$0.1%) in GaAs leads to a large distortion of the conduction band structure: (1) the formation of the lower subband $E_-$ that causes the band-gap energy reduction and (2) the considerable flattening of the lower subband near its minimum leading to a large increase of the electron effective mass.[18,21,23] It has been shown that these N-induced modifications in the conduction band structure lead to over an order of magnitude increase in the *n*-type doping limit in GaAs.[24,25] It has also been demonstrated recently that the band anticrossing model can explain quantitatively the unusual N induced modifications of the conduction band structures of several other III–$N_x$–$V_{1-x}$ alloy systems[7,24–27] as well as some II–VI alloys with some of the anions replaced by small amounts of more electronegative elements.[28]

At present, growth of III–$N_x$–$V_{1-x}$ alloys is considered challenging; bulk material has not been reported and most studies use epitaxial techniques such as gas-source molecular beam epitaxy (MBE) or metalorganic chemical vapor deposition (MOCVD) to grow thin films. In this context, because only a small amount of N (<1%) can lead to a large reduction in the energy band gap of III–$N_x$–$V_{1-x}$ materials, ion implantation is an attractive and feasible alternative approach to synthesize these alloys. Indeed, we have reported preliminary success in forming $GaN_xAs_{1-x}$ and $Al_yGa_{1-y}N_xAs_{1-x}$ alloys by N implantation.[9] In this article we report a detailed optical investigation of $GaN_xAs_{1-x}$, $InN_xP_{1-x}$, and $Al_yGa_{1-y}N_xAs_{1-x}$ alloy thin films formed by N ion implantation.

## II. EXPERIMENTAL DETAILS

Nitrogen ions were implanted into (1) semi-insulating GaAs wafers, (2) InP wafers, and (3) MOCVD-grown 0.3–0.5 $\mu$m thick $Al_yGa_{1-y}As$ epitaxial films on GaAs substrates with $y$ ranging from 0.27 to 0.61. Multiple N implants with energies in the 33–160 keV range were used to create ~2000–3500 Å thick layers with uniform N atomic concentration. The N dose was varied to obtain diluted nitride layers with N concentrations corresponding to N mole fractions of $x_{imp}\approx$0.008, 0.016, 0.018, 0.02, 0.036, and 0.048. All implantations were carried out using a beam current of ~0.2–0.5 $\mu$A/cm$^2$. Further details of the implantation are given in Table I. For the Ga+N coimplanted GaAs samples a 3000 Å thick $SiO_2$ layer was deposited on the GaAs substrate before implantation. Rapid thermal annealing (RTA) was performed on the implanted samples in a flowing $N_2$ ambient in the temperature range of 560–950 °C for 5–120 s with the sample surface protected by either a blank GaAs or InP wafer.

It is important to recognize that only a fraction of the implanted N will become ''active'' by occupying column V sublattice sites after annealing. These ''active'' N atoms will be referred to as N in the group V sublattice $N_V$: e.g., $N_{As}$ for

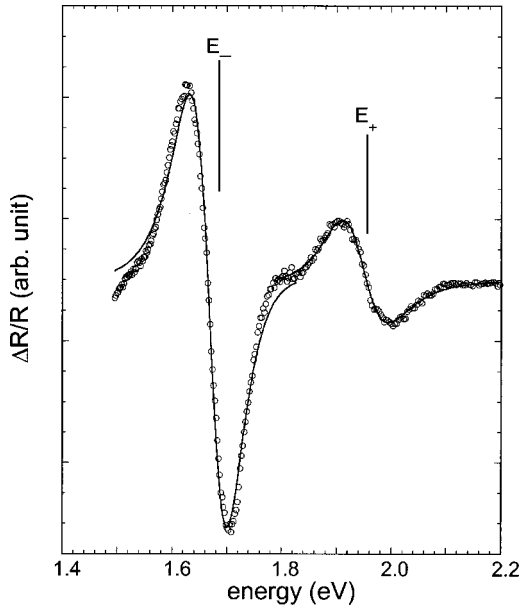


FIG. 1. PR spectrum from a N implanted $Al_yGa_{1-y}As$ ($y=0.27$) thin film ($x_{imp}=0.018$) after RTA at 800 °C for 10 s (open circles). The solid line is a fit to the data according to Eq. (2). The two critical transitions $E_-$ and $E_+$ obtained from fit are also indicated in the figure.

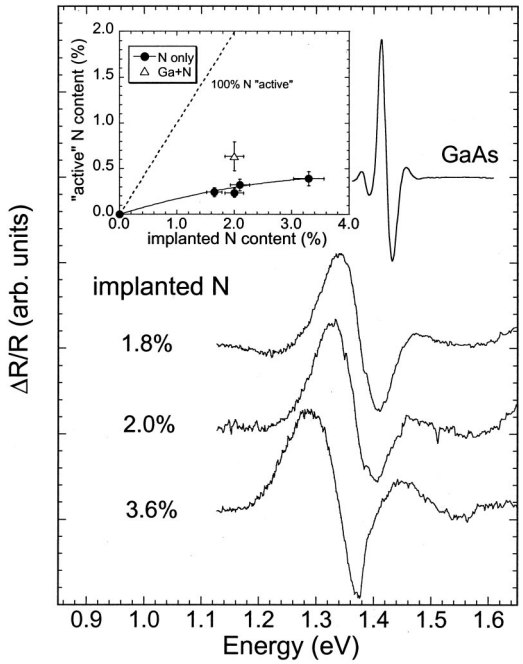


FIG. 2. A series of PR spectra from N implanted GaAs with implanted N doses of 1.8%, 2.0%, and 3.6% after 10 s RTA at 800 °C. The inset shows the mole fraction of N incorporated in the As sublattice calculated from the band-gap reduction as observed by the PR measurements using Eq. (1).

GaAs and $N_P$ for InP. The mole fraction of substitutional N in the group V sublattice will be referred to as $x_{act}$ (i.e., $x_{act} \leqslant x_{imp}$), so that $x_{act}=2[N_V]/n_o$, where $[N_V]$ is the concentration of N in the group V sublattice and $n_o$ is the atomic density of the matrix semiconductor. The activation efficiency is then defined as the ratio of substitutional N in the group V sublattice and the total implanted N, $x_{act}/x_{imp}$.

Photomodulated reflectance (PR) was used to measure the band-gap energy of the samples at room temperature. Quasi-monochromatic light from a halogen tungsten lamp dispersed by a 0.5 m monochromator was focused on the samples as a probe beam. A chopped HeCd laser beam ($\lambda = 4420$ Å) provided the modulation. PR signals were detected by a Ge or Si photodiode using a phase-sensitive lock-in amplification system. The values of the band gap and the linewidth broadening parameter $\Gamma$ were determined by fitting the PR data to the Aspnes third-derivative functional form:[29]

$$\frac{\Delta R}{R} = \mathrm{Re}[Ce^{i\theta}(E - E_{CP} + i\Gamma)^{-n}], \tag{2}$$

where $E$ is the energy of the probe beam, $E_{CP}$ is the critical point energy, $\Gamma$ is a broadening parameter, and $C$ and $\theta$ correspond to the amplitude and phase factors, respectively. For three-dimensional critical point transition, $n$ is taken to be 2.5. Figure 1 shows the PR spectrum (open circles) from a N implanted $Al_yGa_{1-y}As$ ($y=0.27$) thin film ($x_{imp}=0.018$) after RTA at 800 °C for 10 s. The solid line in Fig. 1 is a least-squares fit to the data according to Eq. (2). The two critical transition energies $E_-$ and $E_+$ obtained from the fit are also indicated in the figure.

## III. RESULTS AND DISCUSSION

### A. $GaN_xAs_{1-x}$

Figure 2 shows the PR spectra from an unimplanted GaAs and a series of N-implanted GaAs samples with $x_{imp} \approx 0.018$, 0.02, and 0.036 after RTA at 800 °C for 10 s. The PR spectra shown in Fig. 2 exhibit well-resolved spectral features related to the fundamental band-gap transitions. The significant broadening of the features in the implanted samples can be attributed mainly to the implantation damage. Notice that alloy fluctuation also broadens the transitions. However, PR measurements on MOCVD grown $GaN_xAs_{1-x}$ layers showed only small line broadening for $x<0.01$ (<30 meV).[27] Clearly, the band-gap reduction $\Delta E$ increases with implantation dose in a way analogous to the reduction of the fundamental band-gap energy in $GaN_xAs_{1-x}$ alloys with increasing N content.[2–5] The possibility that the band-gap reduction might be caused by lattice damage created by the implantation was previously investigated.[9] PR measurements on a 200 keV Ga-implanted sample with the total dose of $1\times10^{15}/cm^2$ showed no noticeable shift of the PR transition energies. As expected, the implantation produced a considerable broadening of the PR features as compared to that of the unimplanted GaAs sample. These observations show that, although the lattice damage broadens the spectral features associated with interband transitions, the band-gap reduction in the N implanted GaAs samples is a direct result of the formation of $GaN_xAs_{1-x}$ alloy layers.

The mole fraction of ''active'' N, $x_{act}$ in the ion beam synthesized $GaN_xAs_{1-x}$ layers was derived from the observed $\Delta E$ values by using the band anticrossing model [Eq. (1)], which has been shown to explain very well the dependence of the fundamental band gap on the N content in epi-

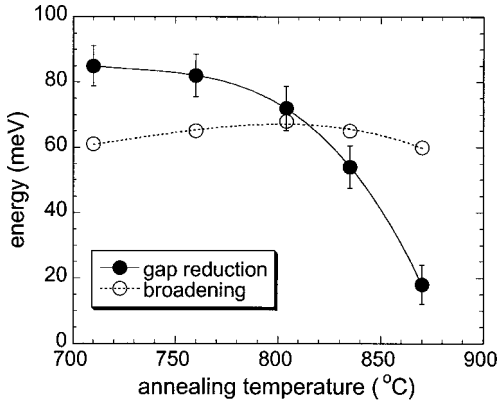


FIG. 3. The band-gap reduction (closed circles) and the line-shape broadening (open circles) from the PR spectra from N implanted GaAs samples with $x_{imp} \approx 0.02$ as a function of 10 s RTA temperature.

taxially grown GaNAs alloys. The results are shown in the inset of Fig. 2. An activation efficiency of about 10%–15% has been achieved for $x_{imp} < 0.036$. The highest $x_{act} \approx 0.004$ has been achieved by N implanting in GaAs with $x_{imp} \approx 0.036$.

The thermal stability of the $N_{As}$ was also investigated. Figure 3 shows the band gap reduction $\Delta E$ from a series of N implanted GaAs samples with $x_{imp} \approx 0.02$ subjected to RTA at between 725 and 870 °C. $\Delta E$ decreases as the RTA temperature increases, especially above 800 °C. In fact, only a negligible band-gap reduction $\Delta E$ (~10 meV) was observed when the RTA temperature was raised to above 870 °C, indicating that less than 0.1% of N remained substitutional in the As sublattice. Secondary-ion-mass spectroscopy measurements showed that the N did not diffuse out of the implanted region even after RTA at 900 °C for 20 s. The results indicate that the substitutional configuration of the $N_{As}$ is thermally unstable. This might be due to the relatively stronger Ga–N bond (6.81 eV) in comparison to the Ga–As bond (5.55 eV) in the Ga–N–As system. Therefore it may be energetically favorable for the N atoms to ''deactivate'' by forming GaN clusters during annealing.

Our recent transmission electron microscopy investigation revealed that in the N implanted GaAs sample after RTA at 950 °C a very high density of small voids, with an average size of about 2 to 3 nm is present in the implanted layer.[30] Such void-like defects are not observed in samples implanted with S and are present only in N implanted samples. This strongly suggests that these voids are related to N and are likely formed by the segregation of N during annealing. Presence of these voids (or N bubbles) may account for the low N activation efficiency in these samples.

We have also attempted to increase the activation efficiency in the N implanted GaAs samples by Ga ion coimplantation. In many III–V semiconductors, coimplantation of a matrix element (e.g., Ga in GaAs) to restore the local stoichiometry has been used successfully to enhance incorporation of electrically active dopants on the opposite lattice sites.[31–35] In the present study, equal amounts of Al or Ga ions were coimplanted with N in GaAs in such a way that their atomic profiles overlapped.

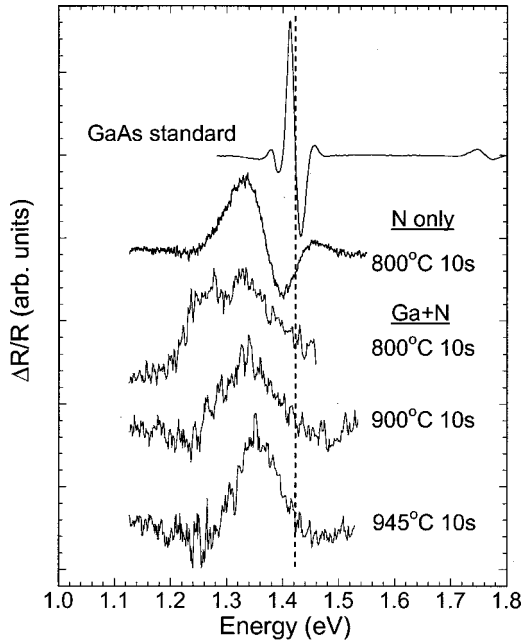


FIG. 4. A series of PR spectra from GaAs samples implanted with N only and Ga+N together after RTA for 10 s in the temperature range of 800–950 °C. For N only implantation, only the PR spectrum from the sample RTA after 800 °C is shown for comparison.

Figure 4 shows a series of PR spectra from GaAs samples implanted with N only and Ga+N coimplanted together with $x_{imp} \approx 0.02$. For samples after RTA under identical conditions we observed a more than a factor of 2 enhancement in the activation efficiency when Ga atoms were coimplanted with N in GaAs. This is apparently due to the creation of a locally nonstoichiometric (Ga-rich) region with a high concentration of As vacancies available for N substitution. After RTA at 800 °C for 10 s, with Ga coimplantation, an $x_{act} \approx 0.0065$ has been achieved (see inset, Fig. 2). Moreover, Fig. 4 also shows that the $N_{As}$ in the $GaN_xAs_{1-x}$ layers formed by Ga and N coimplantation in GaAs are thermally more stable. No $N_{As}$ can be detected after RTA at 950 °C for 10 s for GaAs samples implanted with N alone. When Ga coimplantation was carried out in the same sample, a band-gap reduction of ~70 meV corresponding to an $x_{act} \sim 0.003$ was measured. However, such coimplantation created a highly defective $GaN_xAs_{1-x}$ layer due to the heavy mass of the Ga ions, as is evident in the relatively large values of $\Gamma$ in the PR spectra from the Ga+N coimplanted samples shown in the figure. Therefore the Ga coimplantation method is not suitable for fabricating high quality $GaN_xAs_{1-x}$ layers. Similar enhancement in the N substitution on the As sublattice was also observed when Al atoms were coimplanted with N in GaAs with much less lattice damage (due to the relatively lighter mass of Al compared to Ga). However, since AlGaAs alloys with larger band gap resulted from the Al implantation, no significant net increase in $\Delta E$ was achieved with the Al+N coimplantation.

### B. $InN_xP_{1-x}$

The optical transitions from $InN_xP_{1-x}$ formed by N implantation with increasing N dose in InP after RTA at 800 °C

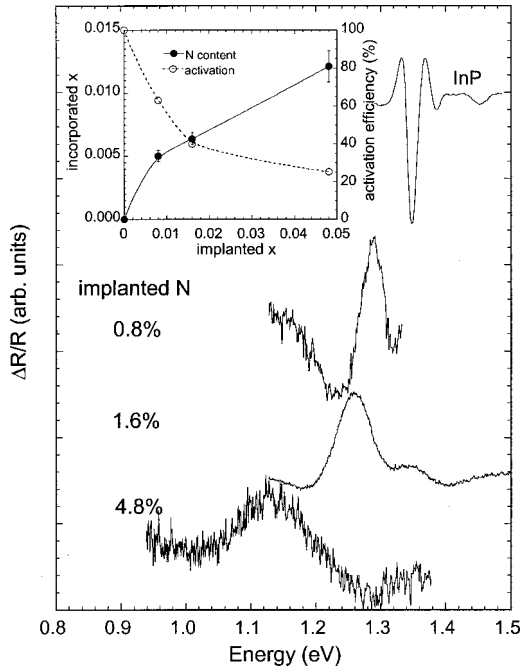


FIG. 5. The PR spectra from N implanted InP with $x_{\mathrm{imp}} \approx 0.008$, 0.016, and 0.048 after 10 s RTA at 800 °C. The inset shows the mole fraction of N incorporated on the P sublattice calculated from the band-gap reduction using the band anticrossing model. The activation efficiencies of N in the three cases are also plotted.

for 10 s are shown in Fig. 5. A monotonic decrease in the band gap is observed as the implanted N dose increases. For the highest implanted N dose corresponding to $x_{\mathrm{imp}} \approx 0.048$ the band gap is estimated to be 1.17 eV, corresponding to $\Delta E = 180$ meV with reference to an unimplanted InP sample ($E_g = 1.35$ eV).

Figure 6 shows the dependence of the band gap of epitaxial $InN_xP_{1-x}$ thin films on the N content $x$ grown by the gas source molecular beam epitaxy (GSMBE) method. The absorption data in the figure are taken from Bi and Tu[8] and the PR data were obtained in the course of this study from $InN_xP_{1-x}$ thin films grown using similar methods.[36] The solid line in Fig. 6 represents $E_-$ calculated by the band

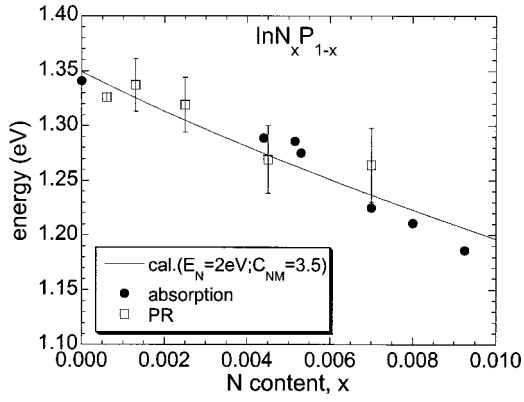


FIG. 6. Band-gap energy as a function of N content in $InN_xP_{1-x}$ alloy thin films grown by GSMBE. The solid line is the calculated dependence of the $E_-$ edge on $x$ according to the band anticrossing model using the known band structure parameters of InP.

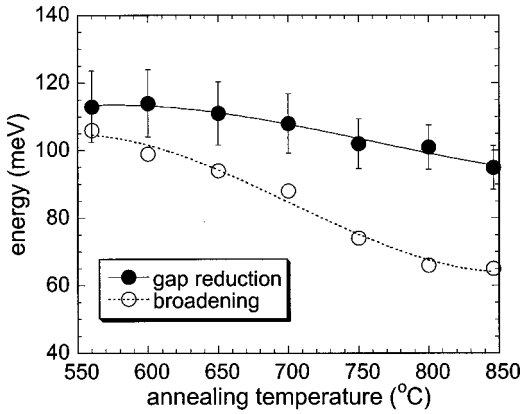


FIG. 7. The band-gap reduction (closed circles) and the line-shape broadening (open circles) from the PR spectra from the $InN_xP_{1-x}$ alloys as a function of RTA temperature.

anticrossing model [Eq. (1)] using the known band structure parameters of the InP matrix, $E_M = 1.35$ eV. The energy of the highly localized nitrogen level $E_N = 2.0$ eV relative to the valence band edge in InP was estimated from the valence band offset $\Delta$eV(GaAs/InP)=0.35 eV. We found that the experimental data in Fig. 6 are best described with a coupling matrix element $C_{\mathrm{NM}} = 3.5$ eV.

Using this fitted parameter we calculated the $x_{\mathrm{act}}$ in $InN_xP_{1-x}$ layers formed by N implantation from the $\Delta E$ values obtained by the PR measurements; the results are presented in the inset of Fig. 5. The amount of N incorporated on the P sublattice $N_P$ in the $InN_xP_{1-x}$ layers was $x_{\mathrm{act}} = 0.005$, 0.0065, and 0.012 for samples implanted with $x_{\mathrm{imp}} \approx 0.008$, 0.016, and 0.048, respectively. Notice that the maximum value achieved for $x$, 0.012, exceeds that reported to date ($x = 0.009$)[8] for $InN_xP_{1-x}$ thin films grown by the GSMBE technique.

It is also important to note in Fig. 5 that the activation efficiency, $x_{\mathrm{act}}/x_{\mathrm{imp}}$ decreases as the amount of implanted N increases. This may be the sign of a limited solubility of N in the InP matrix. For the N implantation dose corresponding to $x_{\mathrm{imp}}$ in the range of 0.01 to 0.02, the activation efficiency is ~40%, much higher than that in N implanted GaAs.

Figure 7 shows the $\Delta E$ and $\Gamma$ values for InP with $x_{\mathrm{imp}} \approx 0.016$ as a function of annealing temperature. Only a small decrease in $\Delta E$ (<20 meV) is observed for the highest annealing temperature used in this study (850 °C), indicating that the N atoms incorporated in the P sublattice are thermally stable. This stands in contrast to the observations with the $GaN_xAs_{1-x}$ layers synthesized by N implantation in GaAs mentioned above, where we have found that the configuration with N atoms substituting As sites is thermally much less stable. Figure 7 also shows the gradual reduction in the linewidth as a function of increasing RTA temperature. This can be interpreted with the removal of implantation defects at higher annealing temperature resulting in improvements of the crystallinity of the implanted layers.

The high activation efficiency and the good thermal stability of N in InP may be due to the small difference between the bond energy of In–N (5.77 eV) and In–P(5.81 eV). The smaller size difference between the N and P atoms compared

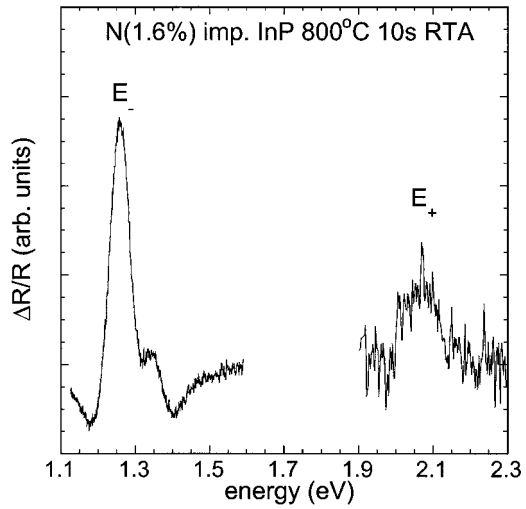


FIG. 8. A PR spectrum from a N implanted InP sample with $x_{\mathrm{imp}} \approx 0.016$ after RTA at 800 °C for 10 s taken over a wide photon energy range showing both the $E_-$ and $E_+$ transitions.

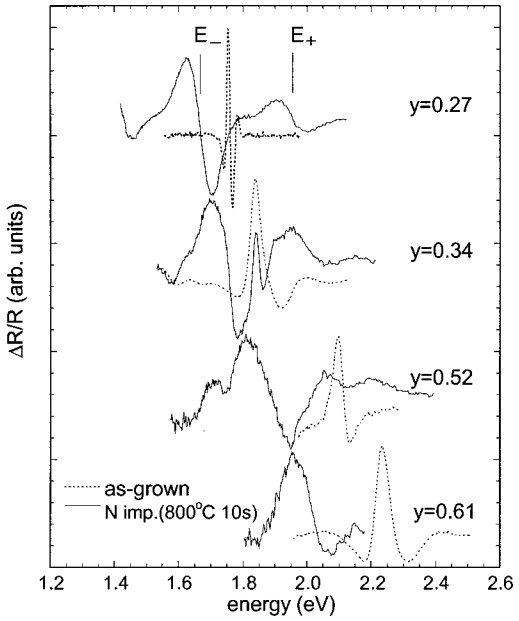


FIG. 9. A series of PR spectra from $Al_yGa_{1-y}As$ samples with various AlAs mole fraction implanted with N ($x_{\mathrm{imp}} \approx 0.018$) after RTA at 800 °C for 10 s (solid lines) together with the spectra of the as-grown materials (dotted lines).

to that between the N and As atoms may also contribute to the improved substitution of N in the P sublattice. In addition to the lower subband $E_-$ that is responsible for the reduction in the fundamental band gap in $III–N_x–V_{1-x}$ alloys, the band anticrossing model also predicts the formation of an upper subband $E_+$. According to the BAC model, the upward shift of this $E_+$ state and the downward shift of the lower $E_-$ state at a given value of $x$ are exactly opposite and equal. PR measurements on epitaxially grown $GaN_xAs_{1-x}$, $Ga_{1-y}In_yN_xAs_{1-x}$, and $GaN_xP_{1-x}$ have clearly showed transitions associated with $E_+$ in agreement with the BAC model.[7,18,19,26,27] Specifically, Perkins *et al.* have shown that $E_+$ in $GaN_xAs_{1-x}$ becomes resolvable from the spin-orbit transition $(E_0+\Delta)$ when $x>0.008$.[19] Since the highest N mole fraction achieved in our ion synthesized $GaN_xAs_{1-x}$ is $\approx 0.004$, $E_+$ is not observable in these samples. In our $InN_xP_{1-x}$ layers formed by ion implantation, the highest $x_{\mathrm{act}}$ is 0.012. Moreover, the large value of $E_N-E_M$ in $InN_xP_{1-x}$ (0.65 eV) indicates that the energy separation between the upper and lower subbands in $InN_xP_{1-x}$ should be much larger than that for $GaN_xAs_{1-x}$ and therefore should be well resolved from the $E_-$ and the spin-orbit transition.

Figure 8 shows a PR spectrum from a N implanted InP sample with $x_{\mathrm{imp}} \approx 0.016$ after RTA at 800 °C for 10 s taken over a wide photon energy range (1.1–2.3 eV). A new PR feature corresponding to the transition associated with the $E_+$ edge is clearly observable at 2.1 eV This transition corresponds to an energy shift from the localized N states $E_+ - E_N = 100$ meV, in perfect agreement with the downward energy shift $E_M - E_- = 100$ meV for this sample. This again confirms that the BAC model provides a quantitative description for the N induced modifications in the conduction band of the $III–N_x–V_{1-x}$ alloy system.

### C. $Al_yGa_{1-y}N_xAs_{1-x}$

Similar to the case of N implanted GaAs, we also observe a significant N-induced reduction of the band gap in N implanted $Al_yGa_{1-y}As$ thin films. Figure 9 shows a series of PR spectra from $Al_yGa_{1-y}As$ samples with increasing AlAs mole fraction implanted with N ($x_{\mathrm{imp}} \approx 0.018$) after RTA at 800 °C for 10 s (solid lines) together with the spectra of the as-grown materials (dotted lines). Positions of both the lower $E_-$ and upper $E_+$ subbands for $Al_yGa_{1-y}N_xAs_{1-x}$ formed by N implantation in $Al_yGa_{1-y}As$ samples determined from the PR measurements in Fig. 9 are shown in Fig. 10 as a function of AlAs mole fraction $y$. Note that the optical transitions to the indirect band gaps at $L$ or $X$ minima are not observed in the PR spectra. The known dependencies of the $\Gamma$, $L$, and $X$ conduction-band minima on $y$ are also shown in the figure. The dependence of the localized nitrogen level $E_N$ on $y$ has been determined from published results on N-related photoluminescence in $Al_yGa_{1-y}As$ alloys doped with N at low impurity like levels. It has been shown that at low temperatures the $E_N$ energy level is located at about 1.69 eV ($y=0$),[22] at 1.87 eV ($y=0.31$),[37] and at 1.9 eV ($y$

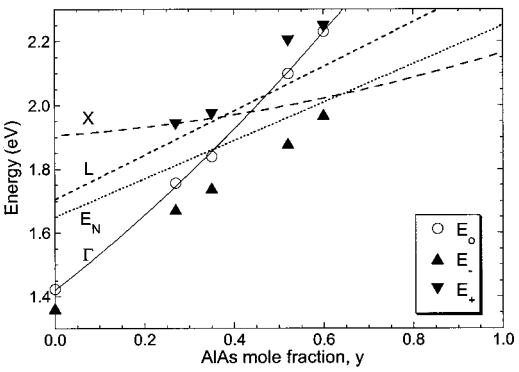


FIG. 10. The $E_-$ and $E_+$ transition energies measured with ion beam synthesized $Al_yGa_{1-y}N_xAs_{1-x}$ samples. The variation of $E_N$ and the $\Gamma$, $X$, and $L$ conduction band edges as a function of AlAs mole fraction in $Al_yGa_{1-y}As$ alloys are also shown.

$=0.37$).[38] This corresponds to a linear dependence of the energy level $E_N$ with the coefficient $dE_N/dy \approx 0.58$ eV. Since the temperature dependencies of the band edge energies are practically the same for all alloy compositions we obtain $E_N = 1.65 + 0.58y$ (eV) for the composition dependence of the N level at room temperature. This dependence is shown by the dotted line in Fig. 10.

It is worth noting that the change of $E_N$ by about 0.58 eV for $y$ changing from 0 to 1 is very close to the valence band offset between GaAs and AlAs, $\Delta E_v = 0.55$ eV. This indicates that the energy $E_N$ is practically constant independent of the AlGaAs alloy composition, a characteristic feature of highly localized levels that has been previously observed for the N-level in GaAsP alloys.[39]

Results in Fig. 10 show an evolution of the $E_-$ and $E_+$ energies as functions of the composition. For GaAs ($y=0$) the wave function of the $E_-$ edge consists mostly of $\Gamma$ edge wave function. This leads to strong optical transitions from the valence band to the $E_-$ subband. On the other hand $E_+$ has mostly the character of the close lying, highly localized N state that only very weakly couples optically to the extended valence band states. In fact the transitions to the $E_+$ states that are clearly discernible in epitaxially grown $GaN_xAs_{1-x}$ films[18,19] were too weak to be observed in N-implanted GaAs. As is seen in Fig. 10 the composition dependence of the relative locations of the interacting $E_N$ and $\Gamma$ levels leads to a change in the nature of the $E_+$ and $E_-$ subbands. At larger $y$ the $\Gamma$ edge moves to higher energies and the $E_+$ subband acquires more $\Gamma$ band-like character. This is reflected in greatly enhanced strength of the optical transitions to the $E_+$ subband (as seen in Fig. 9). At the same time $E_-$ becomes more like a localized N level with decreasing oscillator strength for optical transitions. This Al composition-induced evolution of the anticrossing interaction resembles, as previously observed, a change in the nature of $E_+$ and $E_-$ states with hydrostatic pressure.[18]

Another interesting feature of the results in Fig. 10 is the N-induced transformation of the nature of the fundamental band gap in $Al_yGa_{1-y}N_xAs_{1-x}$. As is seen in Fig. 10 $Al_yGa_{1-y}As$ becomes an indirect gap semiconductor when $X$ shifts below the $\Gamma$ minimum for $y>0.44$. Consequently no PR signal is observed for the lowest band gap for these alloy compositions. However, as is seen for the samples with $y=0.52$ and $y=0.61$ incorporation of a small amount of nitrogen leads to the appearance of direct gap transitions with clearly visible PR spectrum. The direct gap is associated with the transitions to $E_-$ subband that originates from localized N states and partially acquires $\Gamma$-like character through the interaction with the high lying $\Gamma$ band edge. This change in the nature of the fundamental band gap is exactly the same as that recently observed in GaNP alloys.[7] Using the known composition dependence for the $\Gamma$ band edge, $E_M(y)$ and for the localized N level, $E_N(y)$ we can use results for $E_+$ and $E_-$ in Fig. 10 along with Eq. (1) to evaluate the concentration of the active N in samples with different $y$ composition. It has been argued that the value of the coupling parameter $C_{NM}$ depends on the electronegativity difference between nitrogen and the group V element of the host matrix, we can assume that in $Al_yGa_{1-y}N_xAs_{1-x}C_{NM}$ does not depend on the Al composition and is equal to 2.7 eV. From Eq. (1) the mole fraction of active nitrogen in $Al_yGa_{1-y}N_xAs_{1-x}$ can be directly estimated from the energies of $E_+$ and $E_-$. The concentrations of the active nitrogen determined by substituting the results for $E_+$ and $E_-$ shown in Fig. 10 into Eq. (1) are listed in Table II. It is seen that for most Al compositions $0.0018 < x_{act} < 0.003$ which corresponds to the activation efficiency in the range of 10%–16%. The only exception is the sample with $y=0.61$ where a significantly lower concentration of active nitrogen is found. Based on our present results it does not appear that there is any significant dependence of the N activation efficiency on the Al content. The considerable spread in the values of $x_{act}$ for different samples can be attributed to inaccuracies inherent to the ion implantation and thermal activation processes.

TABLE II. Active N $x_{act}$ and the corresponding activation efficiencies calculated from the measured $E_-$ and $E_+$ values for N ion synthesized $Al_yGa_{1-y}N_xAs_{1-x}$ layers using Eq. (1).

| AlAs mole fraction, $y$ | Active N content, $x_{act}$ | Activation efficiency of N (%) |
|---|---|---|
| 0 | 0.0024 | 13.3 |
| 0.27 | 0.0023 | 12.8 |
| 0.34 | 0.0018 | 10.0 |
| 0.52 | 0.0028 | 15.6 |
| 0.61 | 0.001 | 5.6 |

## IV. CONCLUSION

We have successfully synthesized diluted $III-N_x-V_{1-x}$ alloys (with $x=0.002-0.012$) by nitrogen implantation in GaAs, InP, and $Al_yGa_{1-y}As$. Band-gap reductions in the range of 60–180 meV were observed in these ion synthesized $III-N_x-V_{1-x}$ alloys. $InN_xP_{1-x}$ with N contents $x$ as high as 0.012 was synthesized. Both the N activation efficiency and thermal stability of ion synthesized $InN_xP_{1-x}$ alloys were found to be higher than for N implanted GaAs under similar processing conditions. This high activation efficiency and the good thermal stability of N in InP can be attributed to the small difference between the bond energy of In–N (5.77 eV) and In–P(5.81 eV) and the relatively small size difference between the P and the N atoms. Optical investigations on $Al_yGa_{1-y}N_xAs_{1-x}$ layers formed by N implantation in $Al_yGa_{1-y}As$ thin films revealed that the energy shifts of the upper and lower subbands are dependent on the AlAs mole fraction and are in good agreement with the predictions of the band anticrossing model. Moreover, the $Al_yGa_{1-y}N_xAs_{1-x}$ alloys remain direct gap even for $y>0.44$ whereas the band gap of the original $Al_yGa_{1-y}As$ thin films is indirect.

## ACKNOWLEDGMENTS

This work was supported by the ''Photovoltaic Materials Focus Area'' in the DOE Center of Excellence for the Synthesis and Processing of Advanced Materials, Office of Science, Office of Basic Energy Sciences, Division of Materials Sciences under U.S. Department of Energy Contract No. DE-

ACO3-76SF00098. The work at UCSD was partially supported by Midwest Research Institute under subcontractor No. AAD-9-18668-7 from NREL.

[1] M. Weyers, M. Sato, and H. Ando, Jpn. J. Appl. Phys., Part 2 **31**, L853 (1992).
[2] S. Sakai, Y. Ueta, and Y. Terauchi, Jpn. J. Appl. Phys., Part 1 **32**, 4413 (1993).
[3] M. Kondow, K. Uomi, K. Hosomi, and T. Mozume, Jpn. J. Appl. Phys., Part 2 **33**, L1056 (1994).
[4] K. Uesugi, N. Morooka, and I. Suemune, Appl. Phys. Lett. **74**, 1254 (1999).
[5] J. F. Geisz, D. J. Friedman, J. M. Olson, S. R. Kurtz, and B. M. Keyes, J. Cryst. Growth **195**, 401 (1998).
[6] J. N. Baillargeon, K. Y. Cheng, G. E. Hofler, P. J. Pearah, and K. C. Hsieh, Appl. Phys. Lett. **60**, 2540 (1992).
[7] W. Shan, W. Walukiewicz, K. M. Yu, J. Wu, J. W. Ager, E. E. Haller, H. P. Xin, and C. W. Tu, Appl. Phys. Lett. **76**, 3251 (2000).
[8] W. G. Bi and C. W. Tu, J. Appl. Phys. **80**, 1934 (1996).
[9] W. Shan, K. M. Yu, W. Walukiewicz, J. W. Ager, E. E. Haller, and M. C. Ridgway, Appl. Phys. Lett. **75**, 1410 (1999).
[10] M. Kondow, T. Kitatani, S. Nakatsuka, M. C. Larson, K. Nakahara, Y. Yazawa, M. Okai, and K. Uomi, IEEE J. Sel. Top. Quantum Electron. **3**, 719 (1997).
[11] M. Kondow, T. Kitatani, M. C. Larson, K. Nakahara, K. Uomi, and H. Inoue, J. Cryst. Growth **188**, 255 (1998).
[12] D. J. Friedman, J. F. Geisz, S. R. Kurtz, D. Myers, and J. M Olson, J. Cryst. Growth **195**, 409 (1998).
[13] S. R. Kurtz, A. A. Allerman, E. D. Jones, J. M. Gee, J. J. Banas, and B. E. Hammons, Appl. Phys. Lett. **74**, 729 (1999).
[14] L.-W. Wang, L. Bellaiche, S.-H. Wei, and A. Zunger, Phys. Rev. Lett. **80**, 4725 (1998).
[15] E. D. Jones, N. A. Modine, A. A. Allerman, S. R. Kurtz, A. F. Wright, S. T. Tozer, and X. Wei, Phys. Rev. B **60**, 4430 (1999).
[16] T. Mattila, S. Huai-Wei, and A. Zunger, Phys. Rev. B **60**, R11245 (1999).
[17] A. Lindsay and E. P. O'Reilly, Solid State Commun. **112**, 443 (1999).
[18] W. Shan, W. Walukiewicz, J. W. Ager III, E. E. Haller, J. F. Geisz, D. J. Friedman, J. M. Olson, and S. R. Kurtz, Phys. Rev. Lett. **82**, 1221 (1999).
[19] J. D. Perkins, A. Masceranhas, Y. Zhang, J. F. Geisz, D. J. Friedman, J. M. Olson, and S. R. Kurtz, Phys. Rev. Lett. **82**, 3312 (1999).
[20] P. Perlin, P. Wisniewski, C. Skierbiszewski, T. Suski, E. Kaminska, S. G. Subramanya, E. R. Weber, D. E. Mars, and W. Walukiewicz, Appl. Phys. Lett. **76**, 1279 (2000).
[21] W. Walukiewicz, W. Shan, J. W. Ager III, D. R. Chamberlin, E. E. Haller, J. F. Geisz, D. J. Friedman, J. M. Olson, and S. R. Kurtz, in *Photovoltaics for the 21st Century*, edited by V. K. Kapur, R. D. McDonnell, D. Carlson, G. P. Ceasar, and A. Rohatgi (Electrochemical Society, Pennington, NJ, 1999), p. 190.
[22] D. J. Wolford, J. A. Bradley, K. Fry, and J. Thompson, in *Proceedings of the Seventeenth International Conference on the Physics of Semiconductors*, edited by J. D. Chadi and W. A. Harrison (Springer, New York, 1984), p. 627.
[23] C. Skierbiszewski, P. Perlin, P. Wišniewski, W. Knap, T. Suski, W. Walukiewicz, W. Shan, K. M. Yu, J. W. Ager, E. E. Haller, J. F. Geisz, and J. M. Olson, Appl. Phys. Lett. **76**, 2409 (2000).
[24] K. M. Yu, W. Walukiewicz, W. Shan, J. W. Ager III, J. Wu, E. E. Haller, J. F. Geisz, D. J. Friedman, J. M. Olson, and S. R. Kurtz, Phys. Rev. B **61**, R13337 (2000).
[25] K. M. Yu, W. Walukiewicz, W. Shan, J. Wu, J. W. Ager III, E. E. Haller, J. F. Geisz, and M. C. Ridgway, Appl. Phys. Lett. **77**, 2858 (2000).
[26] W. Shan, W. Walukiewicz, J. W. Ager III, E. E. Haller, J. F. Geisz, D. J. Friedman, J. M. Olson, and S. R. Kurtz, J. Appl. Phys. **86**, 2349 (1999).
[27] W. Shan, W. Walukiewicz, K. M. Yu, J. W. Ager III, E. E. Haller, J. F. Geisz, D. J. Friedman, J. M. Olson, S. R. Kurtz, and C. Nauka, Phys. Rev. B **62**, 4211 (2000).
[28] W. Walukiewicz, W. Shan, K. M. Yu, J. W. Ager III, E. E. Haller, I. Miotlowski, M. J. Seong, H. Alawadhi, and A. K. Ramdas, Phys. Rev. Lett. **85**, 1552 (2000).
[29] D. E. Aspnes, Surf. Sci. **37**, 418 (1973).
[30] J. Jasinski, K. M. Yu, W. Walukiewicz, J. Washburn, and Z. Liliental-Weber (unpublished).
[31] R. Heckingbottom and T. Ambridge, Radiat. Eff. **17**, 31 (1973).
[32] K.-W. Wang, Appl. Phys. Lett. **51**, 2127 (1987).
[33] J. Moll, K. M. Yu, W. Walukiewicz, W. L. Hansen, and E. E. Haller, Appl. Phys. Lett. **60**, 2383 (1992).
[34] P. Kringhøj, Appl. Phys. Lett. **64**, 351 (1994).
[35] K. M. Yu and M. C. Ridgway, Appl. Phys. Lett. **73**, 52 (1998).
[36] W. Shan, K. M. Yu, W. Walukiewicz, X. P. Xin, and C. W. Tu (unpublished).
[37] Y. Makita, H. Ijuin, and S. Gonda, Appl. Phys. Lett. **28**, 287 (1976).
[38] S. Gonda and Y. Makita, Appl. Phys. Lett. **27**, 392 (1975).
[39] H. P. Hjalmarson, P. Vogl, D. J. Wolford, and J. D. Dow, Phys. Rev. Lett. **44**, 810 (1980).